Astrophysical Journal, in press April 2002

Bayesian Analysis of Radio Observations of the Be X-ray Binary LS I +61°303

P. C. Gregory

Department of Physics and Astronomy, University of British Columbia, Vancouver, British Columbia, V6T 1Z1, Canada

gregory@physics.ubc.ca

ABSTRACT

The binary star LS I +61°303 is remarkable for its periodic radio outbursts every 26.5 days. We recently discovered a $\sim$ 4.4 year periodic modulation of the phase and amplitude of these outbursts using the Gregory-Loredo Bayesian algorithm for detecting periodic signals of unknown shape. In this paper we obtain improved estimates of both the orbital period (P_1) and modulation period (P_2) based on a larger data set and examine the behavior of the spectral index between 2.2 and 8.3 GHz, versus modulation period. The new estimates are $P_1 = 26.4960 \pm .0028$ days and $P_2 = 1667 \pm 8$ days and our best estimate of the radio phase of periastron is ~ 0.4. Analysis of the spectral index data indicates that the optical depth in the synchrotron emission region is always $<< 1$ at 8.3 GHz, and can reach values ~ 2.7 at 2.2 GHz. A test of the precessing Be star model of Lipunov and Nazin indicates that it is unlikely to be the correct mechanism to explain the 1667 day periodic modulation.

Subject headings: stars:emission-line — radio continuum:stars— Xrays:binaries— methods:data analysis

1. Introduction

The luminous, massive Be X-ray binary, LS I +61°303 (V615 Cas, GT 0236+610) is particularly interesting because of its strong variable emission from radio to X-ray. It is also the probable counterpart to the γ-ray source, 2CG 135+01 (Gregory and Taylor 1978, Kniffen et al. 1997). At radio wavelengths it exhibits periodic radio outbursts with a period

of 26.5 days (Taylor and Gregory 1982, 1984). The X-ray emission (e.g. Taylor et al. 1996, Harrison et al., 2000) is weak (10^{34} erg s^{-1} at maximum) and has been observed to vary by a factor of 10 over one orbital period (Taylor et al. 1996). Paredes et al. (1997) reported an approximately 5 fold 26.7 ± 0.2 day modulation of the 2-10 keV X-ray flux.

In the period 1977 August to 1992 August a total of 12 well defined outbursts, in the frequency range 5 to 10.5 GHz, were recorded by a variety of groups. Beginning in January 1994 (Ray et al. 1997) detailed monitoring was performed (several times a day) with the National Radio Astronomy Observatory Green Bank Interferometer (GBI) at 8.3 and 2.2 GHz. This has yielded high-quality data for an additional 71 outbursts until the GBI monitoring program was terminated in 2000 October 6 due to lack of funding.

The radio outbursts are not stable in phase. Outburst maxima have been seen from phase 0.45 to 0.95, but bright maxima seem to occur near 0.6 (Paredes, Estalella, & Rius 1990). Furthermore the peak fluxes of the outbursts are known to exhibit a long term ~ 1600 day modulation (Gregory et al. 1989, Martí 1993, Martí and Paredes 1995, Peracaula 1997) The recent Bayesian analysis of over 20 years of data (Gregory 1999, and Gregory et al. 1999, hereafter Papers I and II, respectively) clearly demonstrated the existence of a periodic modulation in both the timing residuals (phase) and peak flux density of the outbursts. The peak flux density analysis (paper I) gave a best period of 1632 days and a 68% credible range from 1599 to 1660 days. The combination of the phase and peak flux density yielded a best modulation period of 1584^{+14}_{-11} days. These results were interpreted in terms of variable accretion by a neutron star having an eccentric orbit within the Be star equatorial disk, which exhibits a modulation in the wind speed and or density. Zamanov and Martí (2000) recently demonstrated a modulation on the same time scale, in the EW(H_α) and $\Delta V_{\rm peak}$, the H_α equivalent width and double peak velocity separation, respectively. This latter results strongly suggests that the modulation in the radio emission is related to changes in the disk properties. The saw tooth shape of the derived phase modulation in Gregory et al. 1999, pointed to a rather sudden onset to each new cycle of Be star equatorial disk modulation. That analysis was based on the 57 outbursts available at the time.

In this paper we report our latest analysis of the timing residual and peak flux density for the full 83 outbursts up to the end of the GBI monitoring program. Only outbursts recorded in the frequency range 5 to 10.5 GHz were used in this analysis. We also explore the evolution in the spectral index, α, with P_2 phase and its implications regarding the optical depth of the synchrotron emitting region. The timing residual results provide a powerful way of testing the precessing Be star model proposed by Lipunov and Nazin (1994) to account for the ~ 4.4 year modulation period. The final section contains a summary of conclusions.

2. Data

For the analysis carried out in papers I and II, the data consisted of the times and flux densities of the radio outburst peaks based on an examination of the daily averaged radio flux densities. We used data spanning a frequency range from 5 to 10.5 GHz. The new analysis takes advantage of the longer time base that is available as a result of the latest GBI measurements. For further details about the GBI monitoring program see Waltman et al. 1995 and Ray et al. 1997.

The GBI has both right circular polarization and left circular polarization feeds so that both L-L correlation and R-R correlation flux densities are recorded simultaneously. Towards the end of the GBI monitoring program the receivers were becoming noisier, especially the L-L correlation results. In light of this the L-L and R-R channels were intercompared before averaging, to eliminate one of the channel when it was exhibiting much higher noise than the other. Typically there are approximately 6 measurements per day. A daily average flux density was used for all subsequent analysis.

In this work the times and flux densities of each outburst were based on a cross correlation analysis with outburst templates generated from the GBI data set. Correlation templates were constructed at both 2.2 and 8.3 GHz for three P_2 phase bins, representative of the beginning, middle and end phases of a P_2 cycle. These are shown in Figure 1, together with the spectral index, defined by $S \propto \nu^{\alpha}$, derived from the two frequency templates. The templates were constructed in the following way. The data was first divided into orbits based on our best estimate of the orbital period, P_1, starting from the discovery of the radio emission (Gregory and Taylor, 1977) on Julian Day (JD) $= 2,443,366.775$. Within a given P_2 phase bin a representative outburst was selected and cross correlated with all the other outbursts to obtain alignment delays. The template was then shifted by the indicated delay and scaled in flux to give the closest agreement to the observed outburst. A mean outburst template was then constructed from the shifted and scaled outbursts. This procedure was then repeated using this mean template in a second iteration. Only GBI data were used in the template construction and the number of outbursts in each P_2 phase bin was ~ 27. The templates shown in Figure 1 are based on our final best estimate of the orbital period $P_1 = 26.4960$ days, and the modulation period, $P_2 = 1667$ days.

The 8.3 GHz templates were then applied to all data within the 5 to 10.5 GHz range spanning the 23 years of observations to estimate the outburst times and characteristic flux densities.

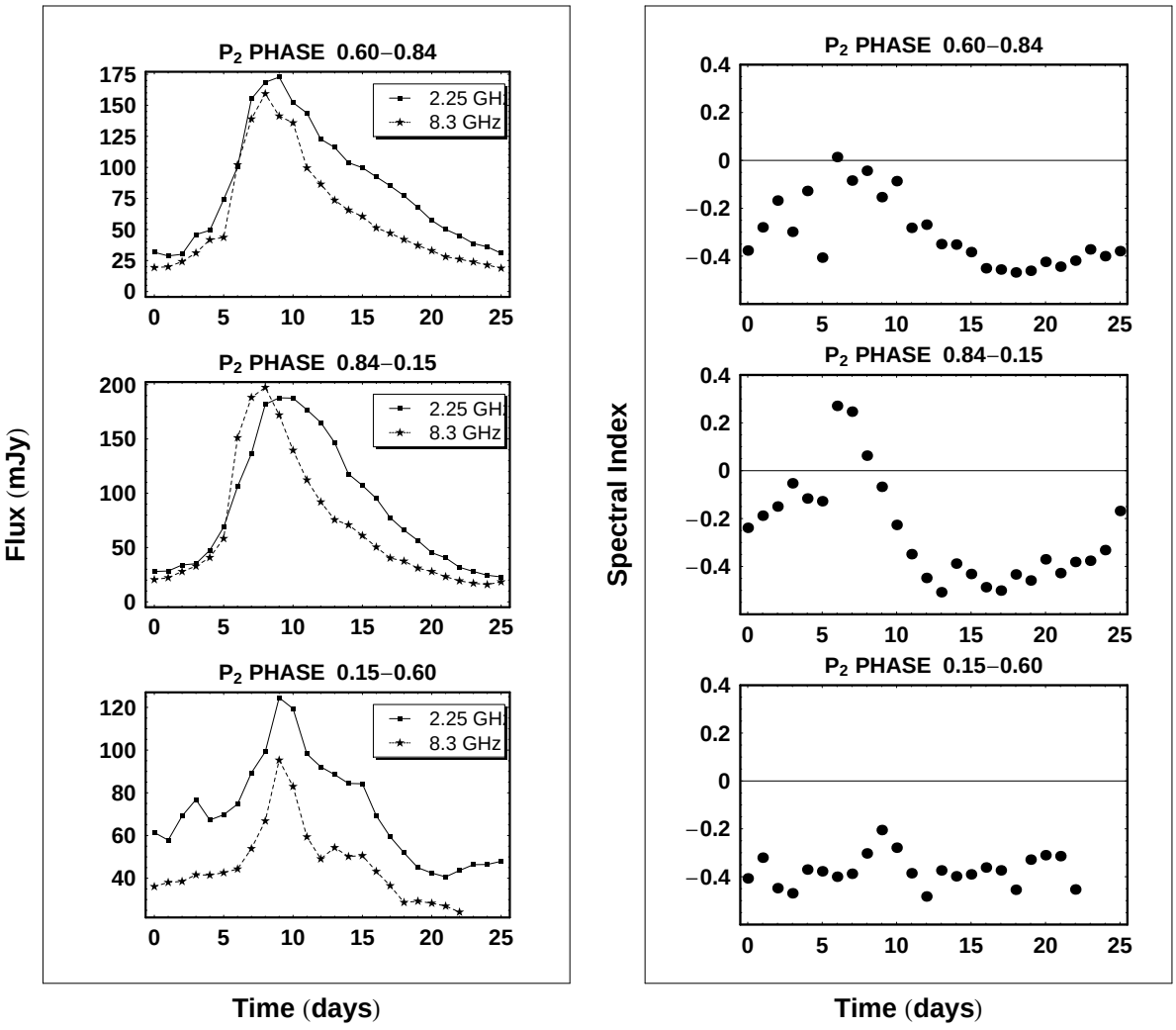

Fig. 1.— The panels on the left show the radio outburst cross correlation templates at 2.2 and 8.3 GHz for three P_2 phase bins. The panels on the right are the 2.2 to 8.3 GHz spectral index templates derived from the cross correlation templates.

3. Results

The outburst times and peak flux densities were processed using a special version of the Bayesian Gregory-Loredo algorithm (Gregory and Loredo, 1992). The GL method is well suited for the detection and measurement of a periodic signal of unknown shape. In (Gregory and Loredo, 1992) details of the theory were presented for the case of a time series where the appropriate noise sampling distribution is the Poisson distribution. In paper I (Gregory 1999) the method was generalized to deal with a time series with independent Gaussian noise. A simple modification of the GL method enables it to handle data sets where the number of periods in the total observing time is small (< 10) and their are significant data gaps. For a detailed discussion of these points see appendix B in Gregory and Loredo (1992) and the appendix of paper I. The current analysis leads to improved estimates of both the orbital period P_1, and the ~ 4.4 year modulation period, P_2. We give results for the shape of the P_2 modulation of the outburst timing residuals, peak flux densities and spectral index. These results are derived from the times and peak flux densities of the outbursts. Using the best estimate of P_1 and P_2 we examine the global properties of the GBI data by constructing intensity plots (flux density versus modulation phase and orbital phase) of the GBI 2.2 and 8.3 GHz daily average flux density and compare with a similar plot of the spectral index data.

3.1. Marginal Probabilities for P_1 and P_2

In the absence of precise knowledge of apastron, we have by convention defined the zero of orbital phase as $\mathrm{JD}_0 = 2{,}443{,}366.775$. This is often referred to in the literature as radio phase. Orbital phase, θ_1, and P_2 phase, θ_2, are given by:

$$\theta_1 = (\mathrm{JD\text{-}JD}_0)/P_1 - \text{Integer part}[(\mathrm{JD\text{-}JD}_0)/P_1], \tag{1}$$

where $P_1 = 26.4960$ days.

$$\theta_2 = (\mathrm{JD\text{-}JD}_0)/P_2 - \text{Integer part}[(\mathrm{JD\text{-}JD}_0)/P_2] \tag{2}$$

Thus θ_1 is a phase which varies between 0 and 1, and similarly for θ_2.

The peak flux density data were analyzed first to derive a marginal probability density of the modulation period, P_2, within a prior period range from 800 days to 2500 days. This is shown in Figure 2(a). A well defined peak was found centered about 1680 days (68 % credible region, 1660-1692 days). A blow up of this peak is shown in Figure 2(b). These results are consistent with our earlier P_2 period determination (68 % credible region, 1559-1660 days) based on a smaller data set of peak flux density data (Paper I).

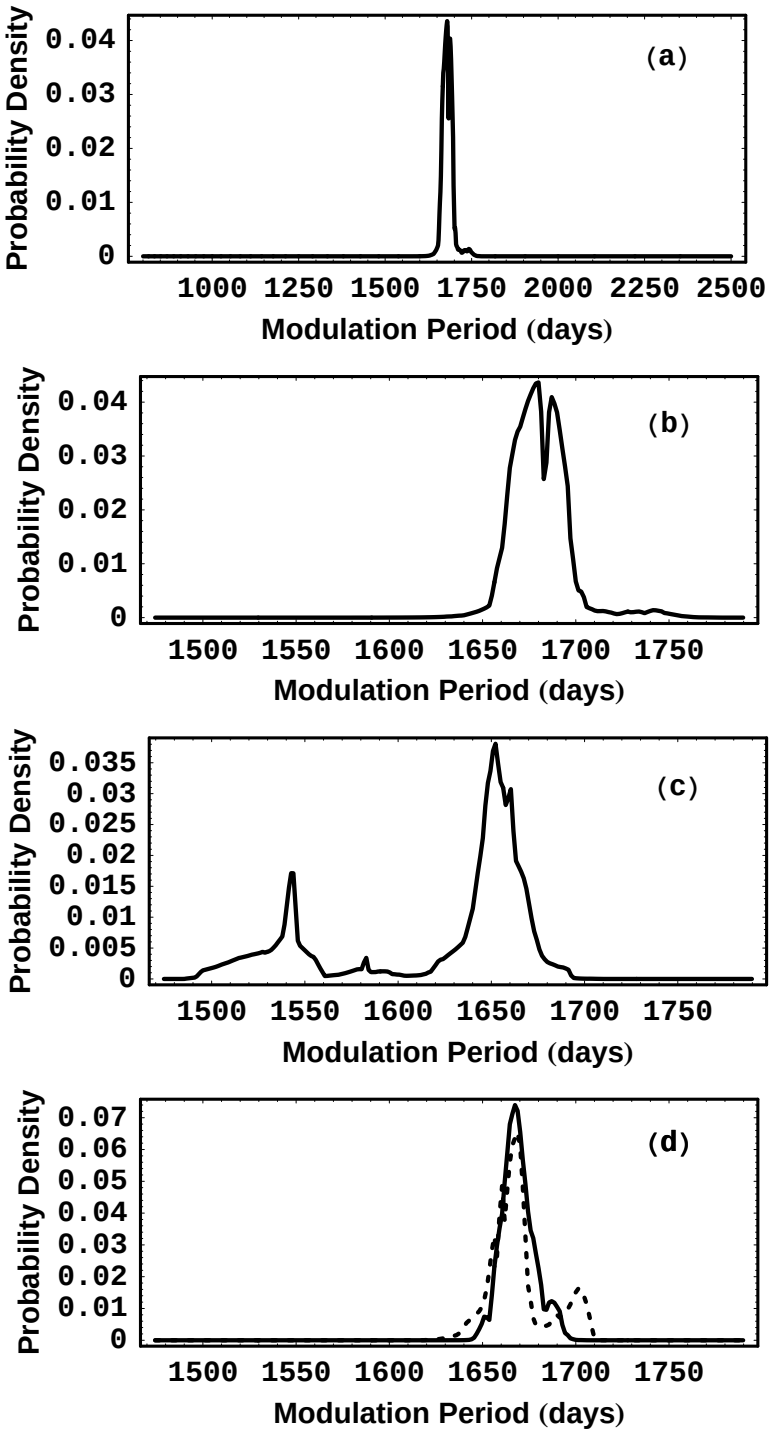

Fig. 2.— Marginal probability of the modulation period. Panel (a) shows the result of the analysis of the outburst peak flux density data. A blow up of the peak region is shown in panel (b). Panel (c) shows the result of the analysis of the timing residuals. The result for the combined analysis of both the peak flux density and timing residual data is indicated by the solid curve in panel (d). The dashed curve is the same but for a simulated data set.

Next the phase of the outburst peaks, derived from the outburst peak times, was separately analyzed. The outburst times were converted to timing residuals after allowing for the orbital period. The details of this procedure were given in paper II. The Gaussian version of the GL algorithm (paper I) was then used to search for any periodicity in the timing residuals, i.e. outburst orbital phase information. Since the same radio data provides the best information about the orbital period, the calculation of timing residuals and the search for a modulation period in the residuals was carried out in a single operation leading to joint probability density function in P_1 and P_2. We computed the timing residuals, τ_i, from $\tau_i = t_i - t_{pi}$. The quantity t_i = the cross correlation estimate of the time of the ith outburst maximum, and t_{pi} = the predicted time of the ith outburst maximum, based on an assumed value of P_1. The value of t_{pi} is given by,

$$t_{pi} = t_0 + P_1 \text{ Nearest Integer}[\frac{t_i - t_0}{P_1}], \tag{3}$$

where t_0 was set equal to t_i for the timing residual reference outburst. To reduce the correlation between the estimates of P_1 and P_2, a timing residual reference outburst [1] was selected that was closest to the weighted mean of all the outburst t_i values (t_0 = Julian Day 2,449,849).

The marginal probability for P_2, shown in Figure 2(c), exhibits a broader range of probability compared to (b) in the range 1500 to 1700 days. The highest peak in the vicinity of 1650 days, is close to the peak found for the flux density modulation. In papers I and II the 68% credible regions (CR) of the two estimates of P_2, based on (a) the peak flux density data , and (b) the timing residuals, were close but did not quite overlap. Nevertheless we proceeded to combine the two probability distributions to arrive at a final best estimate for the marginal probability of P_2. The final result was dominated by the narrow probability distribution associated with the outburst timing analysis, which when compared to Figure 2(c) now appears anomalously narrow.

It is gratifying that with the current larger sample of outbursts and improved cross-correlation estimates of outburst times and peak flux densities, the two 68% credible regions now clearly overlap (compare Figures 2(b) and (c)) and overlap with earlier 68% CR based on the peak flux density data.

Next the timing residual data and flux density data were used in a combined analysis leading to the solid curve in Figure 2(d). Basically the results for (c) were redone assuming (b) as the prior for P_2. This leads to a final best estimate for $P_2 = 1667 \pm 8$ days.

---

[1]The timing residual reference outburst is not the same as JD_0, the reference epoch used for calculation of orbital phase.

Finally we constructed a simulated data set of outburst times and peak flux densities based on sampling the derived periodic timing residual and peak flux density light curves according to the actual sample times and then adding independent Gaussian noise with $\sigma =$ the derived errors in the these two quantities. The simulated data set was processed in exactly the same way as the actual data and resulted in the dashed curve of Figure 2(d). The comparison indicates that any low level structure seen in the solid curve is not the result of the nonuniform sampling but simply due to the effective noise.

In this regard, G. L. Bretthorst (1988, 2001) showed that one great advantage of nonuniform sampling is to increase the effective bandwidth, namely the largest spectral window free of aliases, compared to the same number of uniformly samples in the same time window. The aliasing phenomenon returns at a sufficiently high frequency due to one of the following reasons. (a) The sampling times t_i, although nonuniform, are all integer multiples of some small interval δT, because the times are all derived from some finite clock interval. (b) The data are only recorded to a finite number of decimal places which has the same effect as (a). The effective Nyquist frequency $= 1/(2\ \delta T)$. For our data $\delta T = 1$ day, so aliasing is only expected to be a problem for periods shorter than 2 days.

The marginal probability for P_1 is not shown because of its similarity to Figure 5(b) in paper II. The final result for $P_1 = 26.4960 \pm .0028$ days agrees within the errors with our earlier result of $P_1 = 26.4917 \pm .0025$ days. Due to the variability of the optical spectrum (Gregory et al. 1979), this radio determination of P_1 is our best estimate of the orbital period of LS I $+61°303$.

3.2. Modulation Light-Curves

The Gregory-Loredo algorithm also computes probability distributions for the shape of the outburst timing residual and peak flux density modulation. We present summaries of these multi-dimensional probability distributions in the form of mean $\pm 1\sigma$ light curves. These are shown in Figure 3 versus time. The new data is identified by the box symbol which clearly follows the same pattern as the earlier data identified by the stars.

Spectral index information is plotted versus P_2 phase in panel (c) of Figure 3. The zero of P_2 phase is chosen as JD = 2,443,366.775 by convention, the date of the first radio detection of the star. For each orbit two statistical summaries of the spectral index data were computed: (a) $\alpha_m =$ the median and (b) $\alpha_{pos} =$ an average of the two most positive values (the average of two is simply to reduce the effects of measurement errors). The maximum positive spectral index (between 2.2 and 8.3 GHz) exhibits a sharp rise around

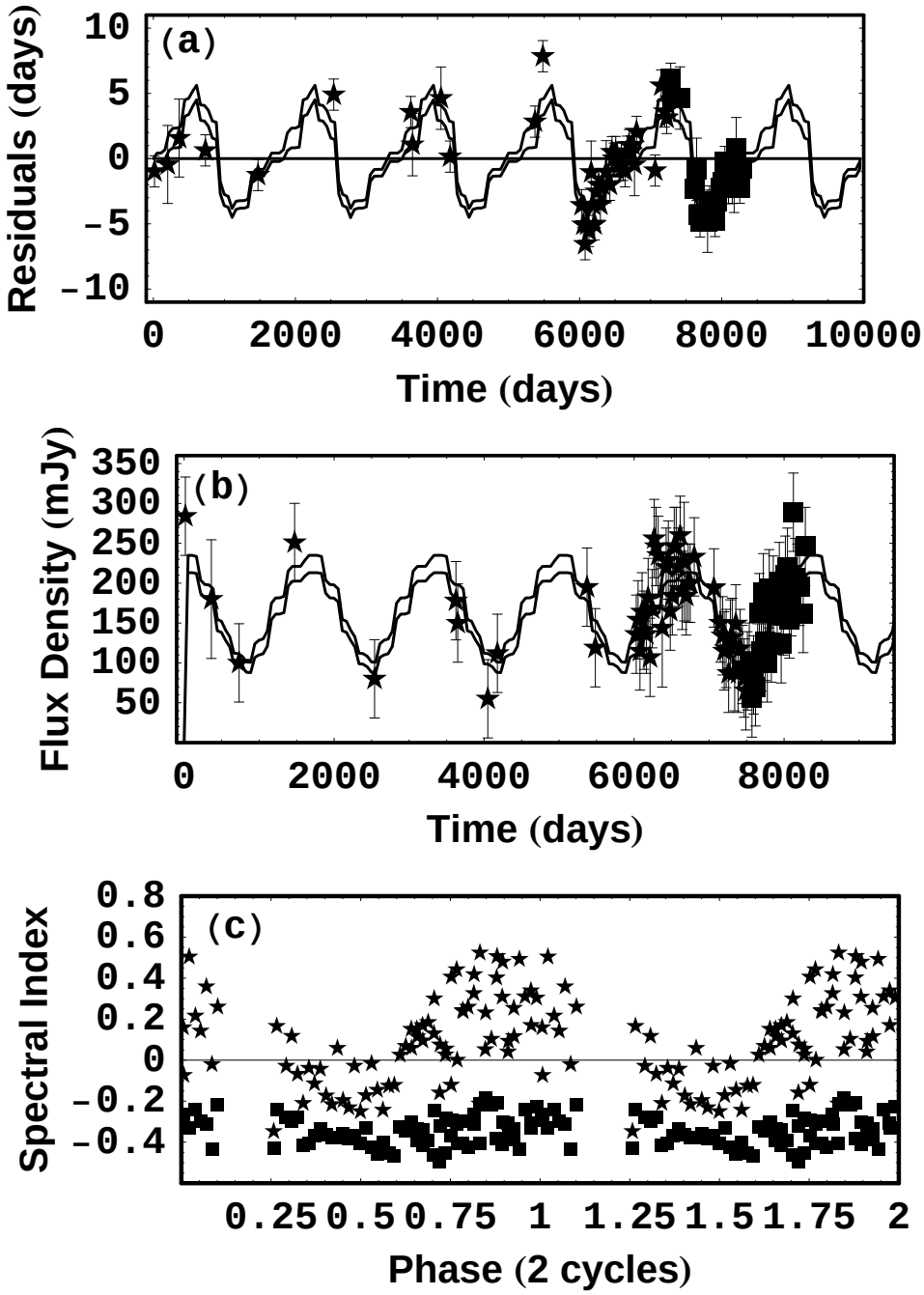

Fig. 3.— Modulation light curves. Panel (a) shows the timing residual light-curve, and panel (b), the peak flux density light-curve, versus time in Julian Days (JD) measured from JD = 2,443,366.775. Panel (c) shows two spectral index statistics versus P_2 phase. The boxes represent α_m = the median spectral index, and the stars represent α_{pos} = an average of the two most positive values.

phase ~ 0.6 and rises to a maximum of $\alpha_{pos} \sim +0.5$ around phase ~ 0.85. Since α_{pos} is an average of the two most positive values it is still quite sensitive to noise peaks and is probably somewhat of an over estimate. The rise in α_{pos} indicates an increase in optical depth of the region producing the synchrotron emission. The median, α_m, remains relatively constant around -0.35. Thus for most of each outburst the spectrum is consistent with optically thin synchrotron emission.

The spectral index information displayed in Figure 3(c) are statistical data for entire orbits. Figure 1 provides statistical information about the variations in spectral index within an orbit for three different choices of P_2 phase range: (1) near the beginning of a cycle, (2) the middle and (3) the end. All three show regions where α reaches a fairly constant level of ~ -0.45, which we interpret as the intrinsic optically thin spectral index. The largest values of α , indicating the highest opacity, occur in the phase range corresponding to the largest outbursts. There α reaches a typical maximum[2] of ~ 0.3. Note a histogram of spectral index values derived from all the 8.3 and 2.2 GHz data exhibits a tail extending to ~ 0.6, but the extremities of the distribution almost certainly reflect the uncertainties in the measured flux densities and thus we believe the spectral index derived from the cross correlation analysis is more realistic.

3.3. Optical Depth Estimates

The spectral index information provides us with additional constraints on the radiating conditions. It is thus useful to estimate the maximum optical depth, τ, of the gas at 8.3 and 2.2 GHz. We have considered three different scenarios.

1. In the first we assume the absorption is due to free-free absorption from thermal gas in the disk between the observer and optically thin synchrotron emitting relativistic gas. As usual we consider the radiating particles to have a power law number density versus energy distribution of the form $N(E)dE \propto KE^{-\gamma}dE$. Here $\gamma = -2\alpha_s + 1 = 1.9$, where $\alpha_s = -0.45$ is the spectral index of the optically thin synchrotron emission defined by $S_\nu \propto \nu^{\alpha_s}$. The absorbing gas is considered to be uniformly distributed in a slab geometry of constant thickness. Although the uniform slab geometry is almost certainly an over simplification, it is sufficient for the back of the envelop estimates of

[2]Our earlier statistical spectral index results (Taylor and Gregory 1982), based on average outbursts at 10.5 and 5 GHz, indicated a larger variation in spectral index. One problem with these earlier results is that the measurements at the two frequencies were widely separated in time.

τ we are seeking here and greatly simplifies the calculations. For this geometry, the ratio of the predicted source flux densities at frequencies ν_1 and ν_2, is given by

$$\frac{S_{\nu_1}}{S_{\nu_2}} = (\frac{S_{\nu_1}}{S_{\nu_2}})_{\tau=0} \frac{e^{-\tau_{\nu_1}}}{e^{-\tau_{\nu_2}}} = (\frac{\nu_1}{\nu_2})^{\alpha_s} \frac{e^{-\tau_{\nu_1}}}{e^{-\tau_{\nu_2}}}, \tag{4}$$

where $(\frac{S_{\nu_1}}{S_{\nu_2}})_{\tau=0}$ is the flux density ratio that would be observed if the free-free optical depth of the slab were zero. $\tau_\nu \propto \nu^{-2.1}$, is the free-free optical depth of the slab, and thus

$$\tau_{\nu_2} = \tau_{\nu_1}(\frac{\nu_1}{\nu_2})^{2.1}. \tag{5}$$

The source exhibited the greatest optical depth when the observed spectral index, α_m, reached a maximum positive value of 0.3. This corresponds to an observed flux density ratio of

$$\frac{S_{\nu_1}}{S_{\nu_2}} = (\frac{\nu_1}{\nu_2})^{\alpha_m}, \tag{6}$$

Substituting equation (5) into equation (4) and equating it to the observed flux density ratio we obtain,

$$\frac{e^{-\tau_{\nu_1}}}{e^{-\tau_{\nu_1}(\frac{\nu_1}{\nu_2})^{2.1}}} = (\frac{\nu_1}{\nu_2})^{\alpha_m-\alpha_s} = (\frac{\nu_1}{\nu_2})^{0.75} \ . \tag{7}$$

We use equations (7) and (5) to estimate the maximum optical depths at 8.3 and 2.2 GHz. They are $\tau_{8.3} = 0.065$ and $\tau_{2.2} = 1.1$.

2. In the second case we consider a uniform slab containing a mixture of synchrotron emitting gas and free-free absorbing thermal gas. In this case equation (4) becomes

$$\frac{S_{\nu_1}}{S_{\nu_2}} = \frac{(j_{\nu_1}/\kappa_{\nu_1})}{(j_{\nu_2}/\kappa_{\nu_2})} \frac{(1-e^{-\tau_{\nu_1}})}{(1-e^{-\tau_{\nu_2}})}, \tag{8}$$

where $\kappa_\nu \propto \nu^{-2.1}$, is the free-free opacity, and $j_\nu \propto \nu^{\alpha_s}$ is the synchrotron volume emission coefficient. Equating equations (8) and (6) and solving we obtain $\tau_{8.3} = 0.17$ and $\tau_{2.2} = 2.7$.

3. In the third case we consider a uniform density slab of synchrotron emitting particles and assume synchrotron self absorption. Equation (8) also describes this case provided we replace κ_ν and τ_ν by expressions appropriate for synchrotron self absorption. In this case $\kappa_\nu \propto \nu^{-\frac{\gamma+4}{2}} = \nu^{-2.95}$, and $\tau_\nu \propto \nu^{-2.95}$. This yields maximum optical depths of $\tau_{8.3} = 0.05$ and $\tau_{2.2} = 2.6$.

We note that in all three cases the maximum $\tau_{8.3} << 1$, while the maximum $\tau_{2.2} \sim 2.7$. Additional support for this conclusion comes from 3 frequency observations (15, 8.3 & 2.2

GHz) of a large outburst on March 1, 1996 ($P_2 = 0.08$) by Harrison et al. (2000). The spectral index between 8.3 and 2.2 GHz becomes positive near the peak of the outburst but the spectral index remains negative between 15 and 8.3 GHz.

3.4. Intensity Plots

The GBI data set provides a wealth of information on a range of time scales about LS I +61°303. In this section we examine one way of obtaining a global view of the daily averaged radio measurements by displaying the individual daily averaged flux density values on a gray scale intensity plot, locating each point according to its orbital phase and modulation phase. The sizes of the dots representing each flux density value is also scaled according to flux density. Gaps indicate an absence of data. Equation (9) defines a term called the P_2 cycle, which represents the number of P_2 cycles that have elapsed since JD = 2,443,366.775.

$$P_2 \text{ cycle} = \frac{(\text{JD-JD}_0)}{P_2} \tag{9}$$

Figure 4 shows the result for both the 8.3 GHz data and 2.2 GHz data. One can clearly see a linear drift in the outburst maxima with P_2 cycle at both wavelengths during both cycles captured in the GBI monitoring program. This bears out the saw tooth shaped timing residual light-curve plot in Figure 3, derived from the much longer run of flux density measurements in the range from 5 to 10.5 GHz, extending back to the discovery of the radio emission in 1977 (Gregory and Taylor, 1978). Each new cycle starts around $\theta_1 = 0.4$ and $\theta_2 = 0.60$. The end of each cycle is much fainter and ceases to be clearly discernable beyond $\theta_1 = 0.9$ and $\theta_2 = 0.45$. The outburst peaks are clearly confined to half the orbit.

Our best estimate of periastron passage is indicated by the horizontal line corresponding to $\theta = 0.4$. This estimate is discussed in section 5 and is based on both the radio and X-ray observations. There is no obvious difference in the location of the dominate ridge of radio emission at the two wavelengths which indicates any delay in the occurrence of the outbursts at 2.2 GHz compared to 8.3 GHz must be ≤ 1 day.

The lower panel in Figure 4 shows a similar plot for the spectral index data, which as expected is much noisier. The brightest points indicate the locations of the largest positive spectral index values. Again a clear ridge is seen between P_2 cycle 3.6 to 4.1. The ridge in the following cycle is discernable but noisier and probably reflects a degradation in receiver performance that was reported towards the end of the monitoring program. The ridge of positive spectral index is clearly shifted earlier by ≈ 0.1 in orbital phase compared to the flux density ridges.

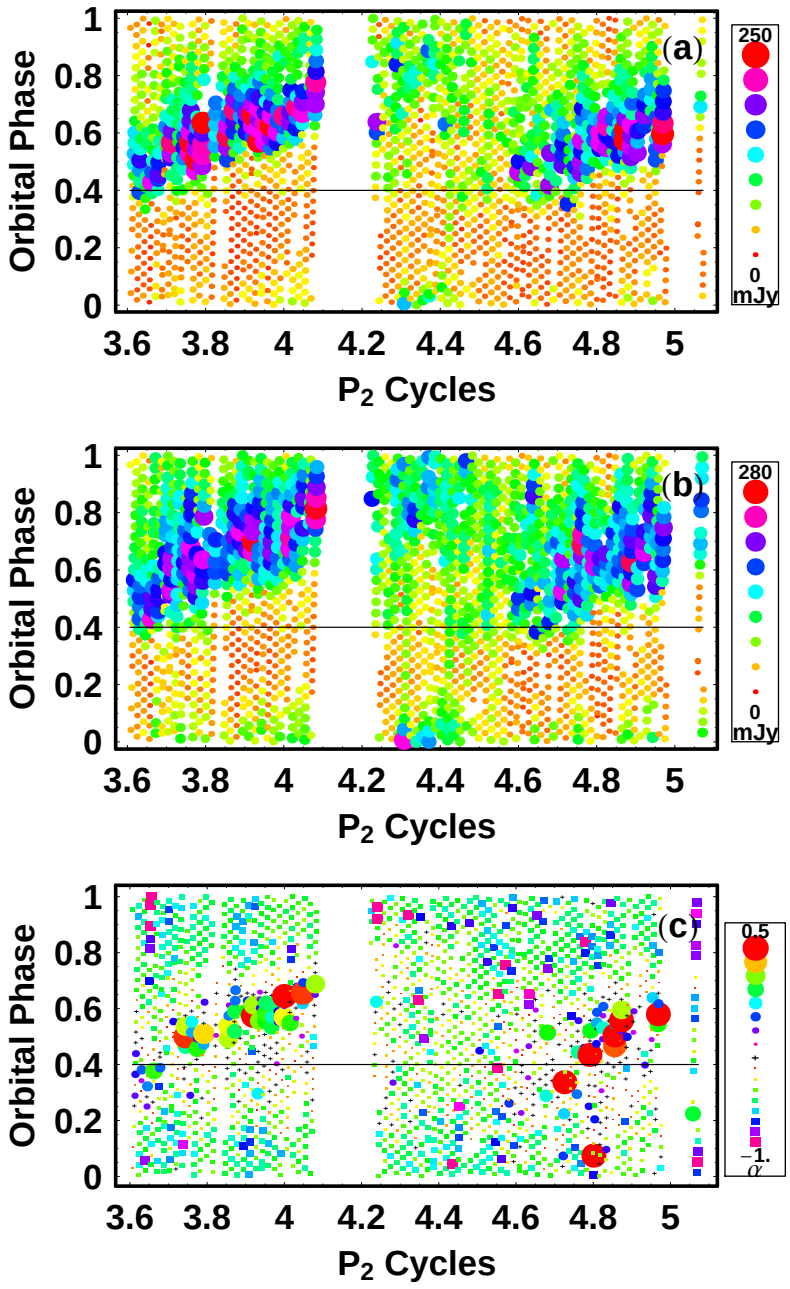

Fig. 4.— Intensity plots of the daily averaged flux densities at, (a) 8.3 GHz, and (b) 2.2 GHz. Panel (c) shows spectral index behavior. The flux density and spectral index are represented by a combination of gray scale and dot size. The larger, darker dots correspond to larger flux densities or more positive spectral indices.

4. Test of the Precessing Be Star Model

According to Hutchings and Crampton (1981) the optical and UV spectra of LS I +61°303 exhibit the characteristics of a rapidly rotating Be star undergoing mass loss through an equatorial disk. Their radial velocity measurements, although difficult to interpret due to the presence of variable emission lines, suggest an eccentric orbit and a period consistent (at the 2 σ level) with the 26.5 day radio outburst period. Existing models (e.g. Maraschi and Treves 1981, Taylor and Gregory 1984, Marti and Paredes 1995, Gregory et al. 1998) to account for the variable radio, infrared and X-ray emission, all invoke a neutron star companion. The outbursts are thought to arise from variable disk accretion by the neutron star. Lipunov and Nazin (1994) have demonstrated that the P_2 modulation period is in rough agreement with the expected period for forced precession of the Be star ($\sim 10^3$ days) in the gravitational field of the neutron star. If true this would require the orbital plane to be inclined with respect to the Be star disk. We will now attempt to test the precession model by comparison with the measurements.

If the two planes are inclined then it follows that the neutron star will intersect the disk plane at two opposite points in its orbit along the line of nodes. Due to precession, the line of nodes will rotate in the orbital plane at a constant angular rate, Ω. If the radio outbursts are associated with accretion of disk material by the neutron star at these intersection points, then it follows that the outburst times will be progressively delayed, assuming the Be star rotation has the same sense as the neutron star orbital motion. For a circular orbit ($e = 0$) the delay would correspond to a constant orbital phase shift per orbit, i.e., $\Delta\theta_1 =$ a constant. Recall from the definition of orbital phase in equation (1), $\theta_1 =$ the fraction of one orbital period. The zero of θ_1 is by convention measured from the orbital position of the neutron star on Julian Day $= 2,443,366.775$, the date of the first radio detection of the star. For an elliptical orbit $\Delta\theta_1$ will vary non uniformly as can be seen from the following argument. The angle through which the line of nodes rotates in one orbital period is a constant $= \Omega\ P_1$. Because the neutron star is moving fastest near periastron it will take a smaller fraction of an orbital period (smaller $\Delta\theta_1$) to move through the angle $\Omega\ P_1$ than at apastron.

In either case we would expect to see two outbursts per orbital period, in contradiction to the one outburst per orbit observed, unless, (a) the true orbital period is twice 26.496 days or 52.992 days, or (b) the disk shadows one of the two outbursts. Based on the available radial velocity measurements (e.g., Hutchings and Crampton 1981), and the analysis of optical and infrared photometry, (e.g., Paredes et al. 1994) the latter period is very unlikely. However, the radial velocity measurements are very difficult to interpret because of the presence of variable emission lines. Out of interest we examined (a) by replotting the GBI radio data as in Figure 4, but with orbital phase based on a 52.992 day period. As expected there are

two outbursts per orbit in this case and each spans a range of 0.25 in orbital phase, or 1/2 the range spanned by a single outburst for an orbital period of 26.496 days. However, the precession model predicts that each outburst will span an orbital phase range of 1.0 in the course of one precession period, in contradiction to the observations.

For case (b), one outburst shadowed, we would expect to see only one outburst per orbit. In one half of a precession period[3] we would see the outburst arising from the passage of the neutron star through the disk in one direction, and in the second half of the precession period we would see the outburst arising from the disk crossing in the other direction. Each would span an orbital phase range of approximately 0.5 in half of a precession period, in keeping with what is observed. How well does this prediction fit the measured orbital phase shift data? We computed the precessing disk outburst phase behavior for both a circular orbit and a wide range of elliptical orbits and compared them with the measurements in Figure 4. We found that a circular orbit gave a bad fit to the data but an elliptical orbit with eccentricity of ~ 0.5 provided a reasonable fit.

There are two problems with the precession model. First, the available evidence (Taylor et al. 1996 and Harrison et al. 2000) indicates that the phase of the X-ray outburst peak is constant around 0.4-0.5 . The precession model provides no natural explanation of this feature in contrast to models which assume the neutron star orbit is coplanar with the Be star disk (e.g., Gregory et al. 1999). Second, for the precession model to work the disk must shadow each of the two outbursts for half of a precession period. We would thus expect to see large optical depths at each end of the phase interval in which a given outburst is visible. We showed earlier in section 3.3 that the optical depth at 8.3 GHz is always $<< 1$ and that the optical depth at 2.2 GHz is a maximum near the middle of the visible orbital phase range of the outburst (see Figure 1), i.e. not at the ends as predicted. For both these reasons we are inclined to rule out the precession model. Since the predicted time scale of precession is the same order of magnitude as the observed modulation period (Lipunov and Nazin 1994), ruling out the model makes it unlikely that disk and orbital plane are inclined.

5. Phase of Periastron

In paper II we outlined how the general properties of the radio emission can be interpreted in terms of the accretion of gas in the Be star equatorial disk by a neutron star in an eccentric orbit embedded in the Be star disk, assuming the gas in the disk has an outward radial component of velocity. This model predicts two accretion peaks, one which occurs

[3]Case (b) requires a precession period of twice 1667 = 3334 days.

at periastron which is associated with the X-ray outburst, and a second peak, associated with the radio outburst, whose orbital phase varies with P_2 phase from close to periastron to apastron.

In terms of this model we can estimate the radio (orbital) phase of periastron passage, θ_{peri}, from the onset of the radio outbursts at the highest observing frequency of 8.3 GHz, for outbursts close to the onset of a new P_2 cycle which occurs around P_2 phase of 0.6 . We obtained estimates of onset times of three well defined outbursts at 8.3 GHz close to P_2 phase of 0.6, where onset is defined by the first data point on the rising portion of the outburst where the flux density is greater than 3 sigma above the minimum. These dates were JD 2,449,443, 2,449,471 and 2,449,498, respectively. They translate to a radio (orbital) phase of 0.33, 0.38, 0.40, respectively, assuming our new best estimate of $P_1 = 26.4960$.

In addition, there have been two simultaneous X-ray and radio monitoring programs that have yielded useful X-ray data on the time scale of one orbital cycle (Taylor et al. 1996 and Harrison et al. 2000). Both found a significant modulation in X-ray emission. The X-ray maxima were located at JD = 48864 ± 3 (P_2 phase = 0.3) and 50161^{+5}_{-1} (P_2 phase = 0.0) which correspond to P_1 radio (orbital) phase ranges of 0.47 ± 0.11 and $0.43^{+.18}_{-.04}$, respectively. Gaps in the X-ray coverage in both observations limit the accuracy of the phase of X-ray maximum. Lower signal-noise ratio X-ray results are also available from the ROSSI satellite all sky monitoring detector (Paredes et al. 1997). They are an average over 10 months of data and phased according to an orbital period of 26.7 days. Correcting these results to an orbital period of 26.4960 days, leads to a periastron estimate of $\theta_{peri} = 0.54 \pm 0.15$. Combining these radio and X-ray estimates yields our best estimate for periastron passage of ~ 0.4. Earlier estimates of periastron (Hutchings and Crampton 1981, Martí and Paredes 1995) range from $\theta_{peri} = 0.2 - 0.5$.

6. Summary

In this paper we have presented improved estimates of both the orbital period (P_1) and modulation period (P_2) of LS I +61°303, based on a larger data set and more accurate estimates of the outburst times and flux densities. We also examined the behavior of the spectral index between 2.2 and 8.3 GHz, versus modulation period. Finally we investigated one proposed mechanism to account for the P_2 modulation period. Our main conclusions are as follows.

1. The new estimate of the orbital period of LS I +61°303 is $P_1 = 26.4960 \pm .0028$ days.

2. The peak radio emission in each orbit occurs somewhere in a range of P_1 radio phase

extending from $\sim$ 0.4 to 0.9. The zero of radio phase is by convention JD_0 = 2,443,366.775, the date of the first radio detection of the star.

3. Periastron passage is estimated from both the radio and X-ray measurements to occur at radio phase of ~ 0.4.

4. The outburst timing residuals, peak flux densities, and spectral index, exhibit a periodic modulation of 1667 ± 8 days. Again by convention the zero of P_2 phase is JD_0.

5. The timing residual light-curve exhibits an approximately saw-tooth waveform suggesting a rather abrupt commencement of each new P_2 cycle around P_2 phase ~ 0.6. At the beginning of each cycle the outbursts occur close to periastron and as the cycle continues the outbursts are progressively delayed reaching apastron around P_2 phase 0.4. Thus the outbursts occur during the outbound portion of each orbit.

6. The outburst peak flux density is a minimum at the end of each P_2 cycle and reaches a maximum around P_2 phase of ~ 0.05 and P_1 radio phase of $\sim 0.6-0.7$ (see Figures 3 and 4). The shape of the peak outburst flux density variations is approximately sinusoidal

7. The spectral index exhibits a marked evolution with P_2 phase. The maximum positive spectral index (between 2.2 and 8.3 GHz) exhibits a sharp rise at the beginning of each P_2 cycle and exhibits a broad maximum extending from P_2 phase ~ 0.78 to 0.05. For most of each outburst the spectrum is consistent with optically thin synchrotron emission with a characteristic spectral index $\simeq -0.45$.

8. The optical depth at 8.3 GHz is always $<< 1$, while the optical depth at 2.2 GHz can reach values of ~ 2.7.

9. The characteristic outburst profiles shown by the cross correlation templates in Figure 1, especially in the lower panel (P_2 phase 0.15-0.6), are very broad and indicate detectable radio emission over the entire orbit. The variations in the optically thin radio emission at 8.3 GHz, may be directly related to variations in the neutron star accretion and thus prove to be a useful probe of the gas density and velocity structure of the Be star equatorial disk.

10. We examined the precessing Be star model proposed by Lipunov and Nazin (1994) to explain the 1667 day modulation period. The model can account for the observed radio outburst phase behavior for an eccentric orbit, provided the disk shadows one of the two expected outbursts per orbit. However, the model does not agree with the observed spectral index behavior and provides no explanation for the observed constant phase of the X-ray outbursts.

The authors wishes to thank Catherine Neish for valuable programming assistance in the preparation of this paper. The Green Bank Interferometer is a facility of the National Radio Astronomy Observatory, which is operated by Associated Universities, Inc., under contract with the National Science Foundation. From 1978-1996, it was operated in support of USNO and NRL geodetic and astronomy programs; after 1996 in support of NASA High Energy Astrophysics programs. This research was supported in part by grants from the Canadian Natural Sciences and Engineering Research Council at the University of British Columbia.

REFERENCES

Bretthorst, G. L. 1988,"Bayesian Spectrum Analysis and Parameter Estimation", Springer -Verlag.

Bretthorst, G. L. 2001, in "Maximum Entropy and Bayesian Methods in Science and Engineering", Joshua Rychert, Gary Erickson and C. Ray Smith (eds.), pp. 1-28, American Institute of Physics.

Gregory, P. C. and Taylor, A. R. 1978, Nature, 272, 704

Gregory, P. C., Taylor, A. R., Crampton, D., Hutchings, J. B., Hjellming, R. M., Hogg, D., Hvatum, H., Gottlieb, E. W., Feldman, P.A. and Kwok, S. 1979, AJ, 84, 1030

Gregory, P. C., Xu, Huang-Jian, Backhouse, C. J., Reid, A. 1989, ApJ, 339, 1054

Gregory, P. C., and Loredo, T. J. 1992, ApJ, 398, 146

Gregory, P. C. 1999, ApJ, 520, 361

Gregory, P. C., Peracaula, M. and Taylor, A.R. 1999, ApJ, 520, 376

Hutchings, J. B., & Crampton, D. 1981, PASP, 93, 486

Harrison, F. A., Ray, P.S., Leahy, D. A., Waltman, E. B., & Pooley, G. C.. 2000, ApJ, 528, 454

Kniffen, D. A. et al. 1997, ApJ, 486, 126

Waters, L. B. F. M. 1987, ApJ, 182, 80

Lipunov, V. M. and Nazin, S. N. 1994, A&A, 289, 822

Martí, J. 1993, PhD theis, Universitat de Barcelona

Martí, J. and Paredes, J. M. 1995, A&A, 298, 151

Maraschi, L. and Treves, A. 1981, MNRAS, 194, 1P

Peracaula, M. 1997, PhD Thesis, Universitat de Barcelona

Paredes, J. M., Estalella, R., Ruis, A. 1990, A&A, 232, 377

Paredes, J. M., Marziani, P., Martí, J., Fabregat, J., Coe, M. J., Everall, C., Figueras, F., Jordi, C., Norton, A. J., Prince, T., Reglero, V., Roche, P., Torra, J., Unger, S. J., and Zamanov, R. 1994, A&A, 288, 519

Paredes, J.M., Martí, J., Peracaula, M. & Ribo, M. 1997, A&A, 320, L25

Ray, P. S., Foster, R.S., Waltman, E. B. et al. 1997, ApJ, 491, 381

Taylor, A. R. and Gregory, P. C. 1982, ApJ, 255, 210

Taylor, A. R. and Gregory, P. C. 1984, ApJ, 283, 273

Taylor, A. R., Young, G., Peracaula, M., Kenny, H. T., and Gregory, P. C. 1996, A&A, 305, 817

Waltman, E., Ghigo, F. D., Johnston, K. J., Foster, R. S., Fiedler, R. L., Spencer, J. H. 1995, AJ110, 290

Zamanov, R. K., and Martí, J. 2000, A&A, 358, L55

This preprint was prepared with the AAS LaTeX macros v5.0.